Complete characterization of laser wakefield acceleration

Laszlo Veisz[*1], Alexander Buck[1,2], Maria Nicolai[3], Karl Schmid[1,2], Chris M. S. Sears[1], Alexander Sävert[3], Julia M. Mikhailova[1], Ferenc Krausz[1,2], Malte C. Kaluza[3,4]
[1] Max-Planck-Institut für Quantenoptik, Hans-Kopfermann-Strasse 1, 85748 Garching, Germany;
[2] Ludwig-Maximilians-Universität München, Am Coulombwall 1, 85748 Garching, Germany;
[3] Institut für Optik und Quantenelektronik, Friedrich-Schiller-Universität, 07743 Jena, Germany;
[4] Helmholtz-Institute Jena, Helmholtzweg 4, 07743 Jena, Germany

ABSTRACT

We report on measurement techniques of the charge, spectrum, divergence, transverse emittance and the first real-time observation of the accelerated electron pulse and the accelerating plasma wave. Our time-resolved study allows a single-shot measurement of the electron bunch duration providing a value of 5.8 +1.9 -2.1 fs full-width at half maximum (2.5+0.8 -0.9 fs root mean square) as well as the plasma wave with a density-dependent period of 12-22 fs. It reveals the evolution of the bunch, its position in the surrounding plasma wave and the wake dynamics. The results afford promise for brilliant, sub-angstrom-wavelength ultrafast electron and photon sources for diffraction imaging with atomic resolution in space and time.

Keywords: Ultrahigh-intensity laser, plasmas, laser-plasma interaction, laser wakefield acceleration, few-cycle laser system, electron acceleration, emittance, electron bunch duration

1. INTRODUCTION

Laser-driven electron acceleration utilizing plasma waves, the so-called laser wakefield acceleration (LWFA) [1] has been proven to generate ultra-relativistic quasi-monoenergetic electron bunches [2][3][4], up to GeV energies [5], down to <1% energy spread [6] with orders of magnitude higher electric fields (100s of GV/m) and much shorter electron pulses (few fs) than state-of-the-art radiofrequency accelerators (100 MV/m, typically ps to ns duration). Although, measurement of the various properties of the electrons is essential for applications, a complete characterization of the LWFA electron sources, in contrast to the radiofrequency sources, is still lacking. The various techniques to obtain the main properties in conventional accelerators such as charge, spectrum, divergence, pointing, normalized transverse emittance, spatial and temporal structure of the bunches or the accelerating field strength and structure are not always adaptable to LWFA. This is due to significant differences in the values of some properties. Therefore, a combination of established and novel methods are required for an in-depth characterization.

Bunch duration measurements up to now have relied on techniques utilizing THz radiation emitted by the electrons while passing through a boundary yielding upper limits for the electron pulse length corresponding to a temporal resolution of ≥ 30 fs [7][8][9][10]. Recently, parallel to our work, few-femtosecond features of the electron pulses have been observed indirectly from the transition radiation spectrum [11]. The plasma wave was observed so far in time-integrating schemes [12][13] incapable of providing insight into the relevant plasma wave dynamics and of timing the accelerated electron bunch with respect to the plasma wave.

We discuss the characterization of the main electron bunch properties in the paper with the emphasis on the detailed temporal measurement of the accelerated electron bunches and the acceleration process itself as it has so far defied accurate determination. We applied the Light Wave Synthesizer 20, an 8-fs optical parametric chirped pulse amplifier system, to generate electrons with 20-30 MeV energy in supersonic He gas jets of few-10^{19} cm^{-3} plasma density [14]. However, the applied techniques are suitable to lasers with longer pulse duration as well. Future applications, such as the development of laboratory X-ray sources with unprecedented peak brilliance or ultrafast time-resolved measurements critically rely on a complete characterization of the acceleration process and the electron bunch.

[*] laszlo.veisz@mpq.mpg.de; phone +49(0)89 329 05-233; fax +49(0)89 329 05-624; www.attoworld.de

Laser Acceleration of Electrons, Protons, and Ions; and Medical Applications of Laser-Generated Secondary Sources of Radiation and Particles, edited by W. P. Leemans, E. Esarey, S. M. Hooker, K. W. D. Ledingham, K. Spohr, P. McKenna, Proc. of SPIE Vol. 8079, 807906 · © 2011 SPIE · CCC code: 0277-786X/11/$18 · doi: 10.1117/12.890952

2. GENERAL CHARACTERIZATION OF ELECTRON BUNCHES

First, a short summary of three former works about characterization techniques for electron bunches originating from laser wakefield acceleration is presented. The purpose of these methods is to determine the charge; the spectrum, pointing and divergence; and the normalized transverse emittance of electron bunches. They are partially based on techniques applied in conventional accelerators, just slightly modified to match the different properties of LWFA electrons.

2.1 Charge[†]

Integrating current transformers are very popular devices in conventional electron accelerators to determine the charge of the electron bunches. They are used in LWFA as well, but their applicability is strongly limited by two facts: the strong electromagnetic pulse (EMP) from the laser-plasma disturbs the results and a very careful shielding is required; and typically a large amount of low-energy thermal electrons with a large divergence are generated together with the monoenergetic electron bunches disturbing or even making it impossible to determine the charge of the peak in the spectrum. A widespread technique to measure the relative –for example in a spectrometer- or absolute charge of laser-driven electron accelerators is the application of scintillating screens as Lanex, Biomax, etc. screens. We have absolutely calibrated eight different screens and performed linearity tests with high dynamic range. The screens have shown a linear behaviour typically over four orders of magnitude and some of them reached a light saturation at the highest applied charge densities. A constant light source was used to simplify the transfer of a one-time absolute calibration to different experimental setups [15].

2.2 Electron spectrum and divergence[‡]

The measurement of energy spectrum in LWFA typically requires a device supporting large electron beam divergence (>1 mrad) and a broad energy range because even when quasi-monoenergetic electron bunches are accelerated their energy can vary and a very significant low energy thermal component might appear in the spectrum. We have designed, constructed and characterized a high resolution, broad energy acceptance spectrometer for laser plasma acceleration experiments [16]. The device contains a permanent magnet with 0.9 T field and an electro magnet with 1.4 T field and is capable to measure in the 2.5-400 MeV energy range. Two different detection systems were implemented: an array of scintillating fiber bundles coupled to a 16 bit CCD having reduced resolution (2.6% at 50 MeV) but very high sensitivity (0.8 fC/channel) and scintillating screens with high spectral resolution (0.5 % at 50 MeV) and extra information about the pointing and divergence in one transverse direction, but reduced sensitivity (about 80 fC). The spectrometer with the screens and 5 mrad electron beam divergence has <2% resolution in the 10-400 MeV range and even <1% above 25 MeV.

2.3 Normalized transverse emittance

The pepper-pot method is one of the usual techniques to measure the transverse emittance of electrons beams in conventional accelerators. The large divergence of LWFA electron beams (typically >1 mrad) compared to rf accelerator beams places additional restrictions on the pepper-pot design. This method was applied to measure the transverse emittance of quasimonoenergetic electrons with 20 MeV energy produced by LWFA in a single shot and a compact setup [17]. A thin (200 μm) tungsten mask with a narrow slit (20 μm) structure was placed into the electron beam path and the profile of electron beamlets was measured in a certain distance with a Ce:YAG scintillator crystal imaged onto a CCD. From the details of the pattern integrated in one direction and the geometry of the setup the geometric emittance was determined. The electron spectrum was observed -with a reduced resolution- during the emittance measurement. As the geometric emittance was found to be inversely proportional to the electron energy, the transverse normalized emittance was constant. The results showed a normalized rms transverse emittance of the LWFA beam of $\varepsilon_N \sim 2.3\ \pi$ mm mrad, with a shot-to-shot fluctuation of 17%. This emittance is comparable to state-of-the-art injectors for conventional linear accelerators.

[†] In cooperation with K. Zeil, A. Jochmann, S. D. Kraft, J. Pawelke, R. Sauerbrey, T. Cowan, U. Schramm – *Helmholz Zentrum Dresden Rossendorf*; A. Popp[1,2], S. Karsch[1,2]; B. Hidding, T. Kudyakov – *Heinrich-Heine-Universität Düsseldorf.*

[‡] In cooperation with Sofia Benavides Cuevas[1], Dieter Habs[2], Ulrich Schramm – *Helmholz Zentrum Dresden Rossendorf.*

3. DIRECT TEMPORAL OBSERVATION OF LASER WAKEFIELD ACCELERATION

In this chapter we present snapshots of the magnetic field generated by the accelerated electron bunch and simultaneously of the plasma wave by the combination of two techniques: time-resolved polarimetry [18][19] and plasma shadowgraphy [20]. The experiments were performed with the LWS-20 producing 8-fs pulses with peak powers up to 16 TW at a carrier wavelength of 800 nm [21]. In the current study, LWS-20 delivered 8.5 fs (FWHM) pulses with an energy of 65 mJ on target. The ultra-short laser pulses were focused onto a supersonic He gas jet with a f/6 off-axis parabola to a spot size of 7.2 µm FWHM and a peak intensity of $I_{peak} = 6x10^{18}$ W/cm^2 ($a_0 = 1.67$) to accelerate electron bunches via self-injection in the bubble / blow-out regime. The electron bunches exhibited a quasi-monoenergetic spectrum of $E_{peak} = (19.2 \pm 6.7)$ MeV, an energy spread of $\Delta E = (2.3 \pm 1.9)$ MeV (FWHM), a divergence of (10.9 ± 3.5) mrad (FWHM) and carried a charge of $Q = (2.3 \pm 1.8)$ pC in a setup similar to that described in [14]. A 2-mJ probe pulse was split from the beam through a hole in one of the plain mirrors before focusing and directed onto the gas jet perpendicularly to the main beam (Fig. 1).

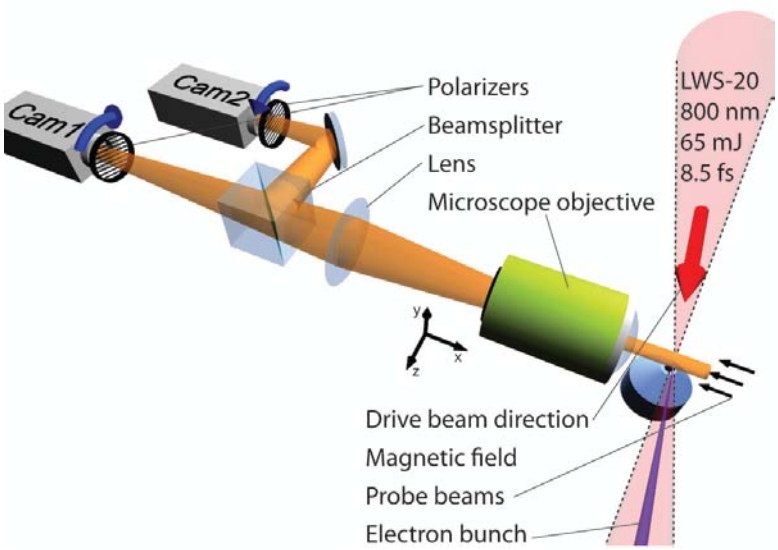

Figure 1. Experimental setup for the temporal investigation of laser wakefield acceleration. Polarimetry and shadowgraphy are implemented using the same probe beam. Electrons are accelerated by the drive laser beam (red arrow) out of a supersonic gas jet with a flattop density profile from a de Laval nozzle with 300 µm exit diameter (blue). The probe beam (black arrows) propagates perpendicularly to the main beam through the plasma. In the vicinity of the electron bunch the polarization is rotated by φ_{rot} as a result of the Faraday effect (see equation (1)). The interaction region with the plasma wave is imaged to two CCD cameras. In front of the cameras are two Glan-laser polarizers with high extinction ratios, which are rotated (blue arrows) away from extinction of the probe beam in opposite directions by ±7°. The shadowgrams are recorded simultaneously with both cameras.

3.1 Polarimetry

Sub-10-fs polarimetry is based on the probe pulse undergoing polarization rotation due to the Faraday effect caused by the component of the azimuthal magnetic field, generated by the trapped relativistic electron bunch, parallel to the k-vector of the probe (see Eq. 1). The angle of rotation caused by this magnetic field localized around the electron bunch is

$$\varphi_{rot} = \frac{e}{2m_e c n_c} \int_l n_e \vec{B}_\varphi d\vec{s} \,, \qquad (1)$$

where $\mathbf{B}_\varphi$ is the azimuthal magnetic field surrounding the electrons, e, m_e,n_e, c and n_c the electron charge, electron mass, density, vacuum speed of light and critical density (here: $n_c = 1.76x10^{21}$ cm^{-3}), and d**s** a path element along the path l of the probe through the plasma. Comprehensive numerical simulations [22] indicated that both the electron density of the bunch and the magnetic field caused by the moving electrons have the same duration and further magnetic fields inside the bubble, generated by the displacement current, are by a factor of 7 smaller and have a negligible effect on the

longitudinal extension of the region with rotated polarization [23]. The location, duration and charge of the electron bunch can be inferred from the measurement of the rotation angle φ_{rot} in the transverse (y,z) plane (see Fig. 1) because of the uniquely short probe pulse used. The rays of the probe beam passing the electron bunch above or below the laser axis are rotated in opposite directions. For a sensitive, low-background measurement of φ_{rot}, this region was imaged onto two CCD cameras by using a non-polarizing beam splitter behind the imaging lenses (Fig. 1). Polarizers in front of the CCDs were rotated away from extinction of the original probe beam polarization in opposite directions by (7.0±0.3)°, slightly greater than the expected rotation angles. Thus, the intensity in the images is modulated and regions with positive or negative polarization rotation seem brighter on one camera than on the other. The rotation angle φ_{rot} can be deduced by inversion of the intensity ratio of the two images. A result from an inversion is shown in Fig. 2 [23].

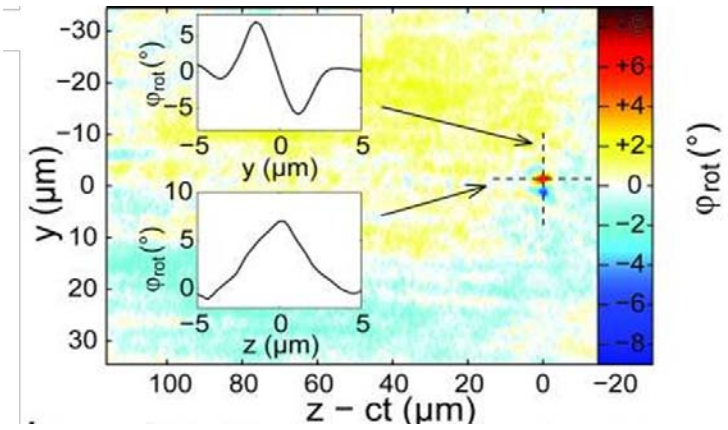

Figure 2. Visualization of the electron bunch. Polarization rotation angle of the probe beam due to the Faraday effect. Insets: Transverse and longitudinal lineout of the rotation angle.

3.2 Shadowgraphy

Sub-10-fs shadowgraphy provides insight into the structure of the plasma wave accelerating the electrons by density-dependent deflection of the probe beam. The rays of the probe beam are deflected as they traverse the plasma wave, depending on the electron density gradient, as illustrated in Fig. 3 left upper panel. This leads to an intensity modulation of the probe beam in the plane at the centre of the plasma wave with the same periodicity. Imaging this plane using a camera with a high resolution and thus small depth of focus in turn shows the modulation as a shadowgram of the plasma wave on the camera. The modulation is not averaged out, because the probe pulse duration is shorter than half the plasma period, the spatial resolution is much higher than the plasma wavelength and the depth of focus is small compared with the transverse size of the plasma wave. The modulation depth is proportional to the amplitude of the nonlinear plasma wave as indicated in Fig. 3 left lower panel. Although, the measured oscillations are smoothed owing to limited resolution and do not reflect the strong nonlinearity of the real plasma wave, they still reflect its original period and position. To obtain firm evidence for the origin of the observed oscillations, we measured their period as a function of electron density while all other experimental parameters were kept constant (Fig. 3 right panel). The period of the plasma wave -in the non-relativistic limit- is given by

$$T_{plasma}=2\pi\sqrt{\frac{\varepsilon_0 m_e}{e^2 n_e}}\,, \qquad (2)$$

where ε_0 is the vacuum permittivity, plotted as red line in Fig. 3. The good agreement of the time-resolved plasma oscillation period with equation (2) corroborates that the oscillations originate from the plasma wave and reveal that the period is not significantly elongated by relativistic effects under our experimental conditions, which is supported by simulations also. Although, the unparalleled spatio-temporal resolution of our probing makes plasma dynamics and accelerated electron bunching directly observable for the first time, this resolution still has to be further improved to unravel details of these dynamics such as non-sinusoidal plasma oscillations.

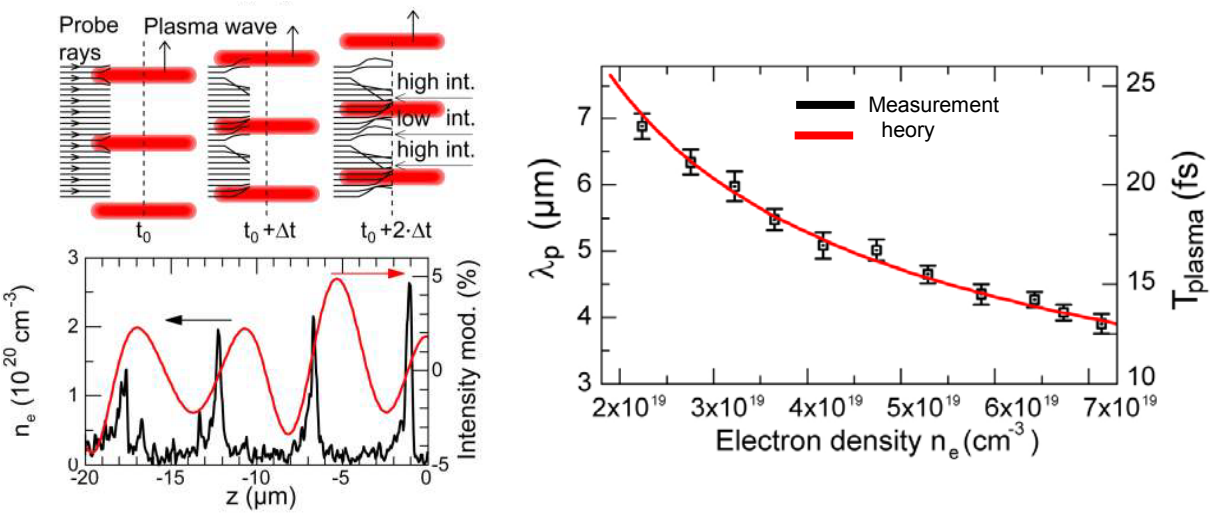

Figure 3. Left upper panel: Refraction of the probe beam (black rays) at the high density peaks of the plasma wave (red bars) at three instances in time. The probe beam is refracted already in the first half (transversely) of the plasma wave leading to a modulated intensity of the probe beam in the imaged plane (dashed line). Left lower panel: Imaging this plane with a high resolution produces an intensity modulation on the camera (calculated with finite pulse duration and spatial resolution, red line) as a signature of the plasma wave (lineout from PIC simulations, black line). Right panel: Plasma wavelength/period versus electron density. Error bars are one standard deviation combined with scaling uncertainty. Each point is an average of 4–7 shots. The red line shows the theoretical non-relativistic plasma period (Eq. 2).

3.3 Results and discussion

The electron pulse duration can be directly inferred from the polarization rotation signal (Fig. 2). Averaging over 85 shots, the rotation signal seems to have a longitudinal extent of φ_{rot} = (3.8±0.2) µm (FWHM), which is the convolution of the bunch length with the probe pulse duration, the transverse size of the azimuthal magnetic field (that is the transit time of the probe beam through the electron bunch) and the imaging resolution. A careful deconvolution of the longitudinal extent yields a mean FWHM electron bunch duration of τ_{bunch} = 5.8 +1.9 -2.1 fs (2.5 +0.8 -0.9 fs root mean square), which is in excellent agreement with the simulated value. The simulation shows that contributions to the region of rotated polarization from the electrons constituting the plasma wave at the bubble vertex cannot be neglected. Consequently, the actual bunch duration is expected to be even shorter than the result of our above analysis.

Lineouts from raw images of camera 1 (see Fig. 1) combined with the polarization rotation signal at various time delay values between the main laser pulse and probe beam are plotted in Fig. 4 left panel. This allows snapshots at various stages of the acceleration and thus tracking the evolution of the electron bunch and the plasma wave. The plasma wave trailing the laser pulse and the electron bunch -visualized by shadowgraphy (Fig. 3)- is visible to the left of the region with rotated polarization. The first polarization rotation signals are detected after a propagation distance of the laser pulse of 190 µm in the gas jet, see Fig. 5. The mean duration of the polarization rotation signal and the deconvolved electron bunch duration are shown in Fig. 4 right upper panel for each delay step, that is, each position inside of the plasma. It can be seen that the bunch duration is constant within the error bars, showing an upper limit of 7-8 fs (FWHM). Also plotted is the peak polarization rotation angle (Fig. 4 right middle panel), which is proportional to the beam current. The nearly constant bunch duration and peak rotation angle imply that the total injected charge remains constant in the last third of the gas jet. The vanishing of φ_{rot} for z < 190 µm and its reaching a maximum at about z = 220 µm, in combination with a nearly constant bunch length, indicates that injection is confined to a propagation length of about 30 µm close to z = 200 µm downstream from the entrance of the plasma channel. Over approximately the same longitudinal range, the accelerating plasma wave exhibits a decrease in total length as well as in its amplitude that is proportional to the modulation depth of the probe intensity variations (Fig. 4 right lower panel). This reduction in the plasma wave amplitude is caused by the injected and accelerated electrons. These electrons do not contribute to the longitudinal

electric field but gain energy from the plasma wave and damp it. Both observations are consistent and indicate that our approach provides real-time access to the electron injection and trapping process of a laser-driven plasma accelerator. As no polarization rotation signal is observed before z = 190 µm, where the plasma wave amplitude is larger, the contribution to the magnetic field of the displacement current is indeed negligible for the measurement, as also indicated by the simulation.

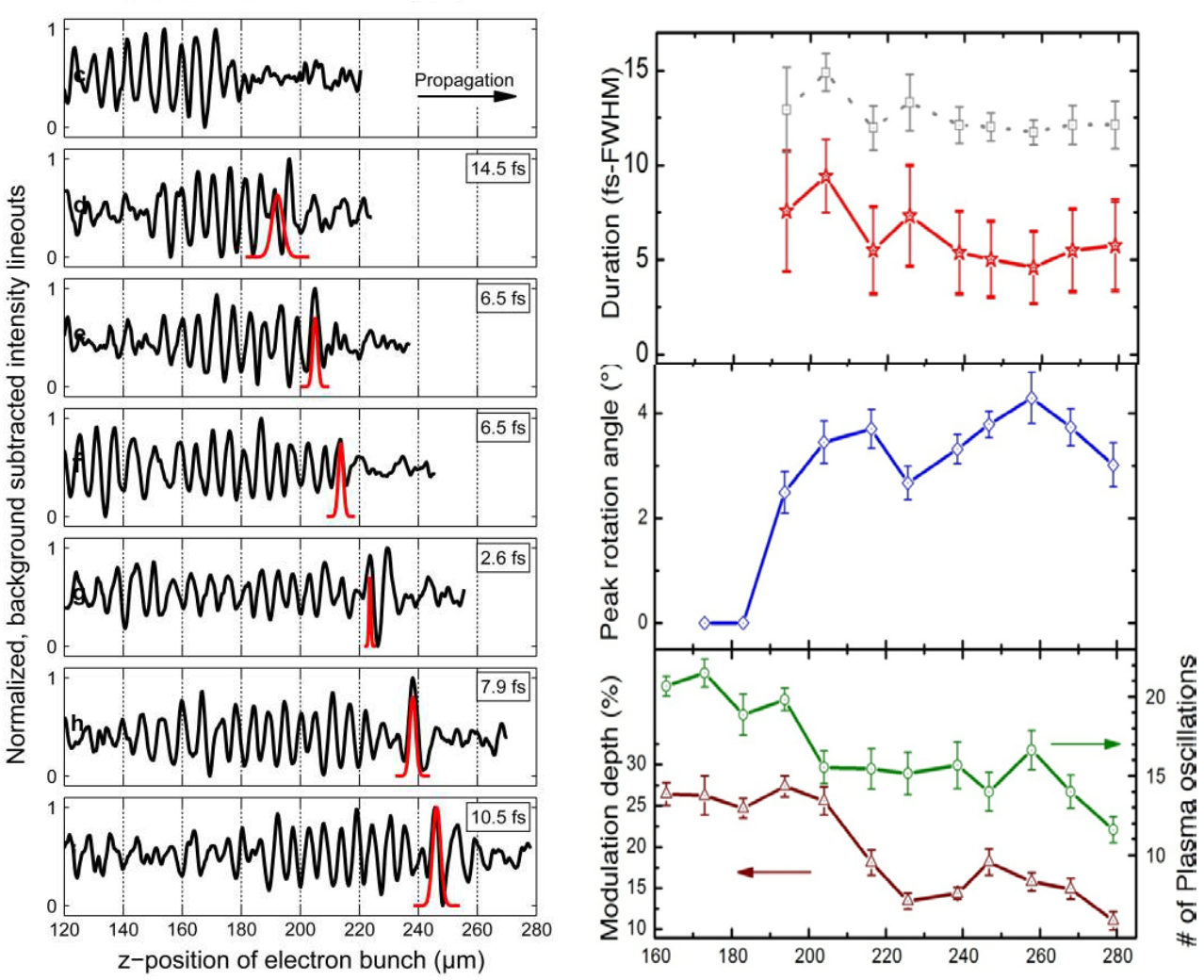

Figure 4. Evolution of the electron bunch and the plasma wave during the acceleration process. Left panel: Representative lineouts along the laser propagation axis (slightly tilted to the *z* axis) of the intensity modulation due to probe beam refraction at the plasma wave (black line) and position and duration of the deconvolved electron pulse duration (red line) for different delay steps. The background plasma density is 3.2×10^{19} cm^{-3}. The plasma wave is detected in all shots at a particular delay, however the modulation visibility and apparent length fluctuate from shot to shot. Shots where both the plasma wave and the electron bunch are clearly visible were selected for these lineouts. The given pulse durations for each shot are not representative of the average pulse duration at this position. Uppermost lineout: Shows the plasma wave at *z*=183 µm, where no polarization rotation due to an injected electron bunch is detected. Right upper and middle panels: Evolution of the deconvolved FWHM electron pulse duration (red stars), the original duration of the polarization rotation (grey squares) and the peak polarization rotation angle (blue diamonds) during the propagation through the plasma. Each point is an average of 4–22 measurements, error bars are 1 s.d. Right lower panel: Simultaneous evolution of the number of identifiable plasma oscillations in the raw images, (green circles) and the intensity modulation depth (brown triangles) in the shadowgraphy images. Each point is an average of five measurements, error bars are one standard deviation.

The measurement curves in Fig. 4 right panel indicate only one electron bunch in the accelerator within the measurement limits. The intensity modulation is visible only behind the Faraday rotation signal, except for one maximum caused by the electrons that are being pushed forward by the laser, which can appear in front of the electrons in some shots. This reveals that the accelerated main electron bunch is trapped inside the first plasma wave oscillation, in agreement with our simulation as well as earlier experiments. From the large number of plasma oscillations (typically 10-20), we learn that the plasma wave does not decay completely after the first wake. This indicates that the wake is not heavily loaded, as this would lead to rapid destruction of the subsequent plasma oscillations.

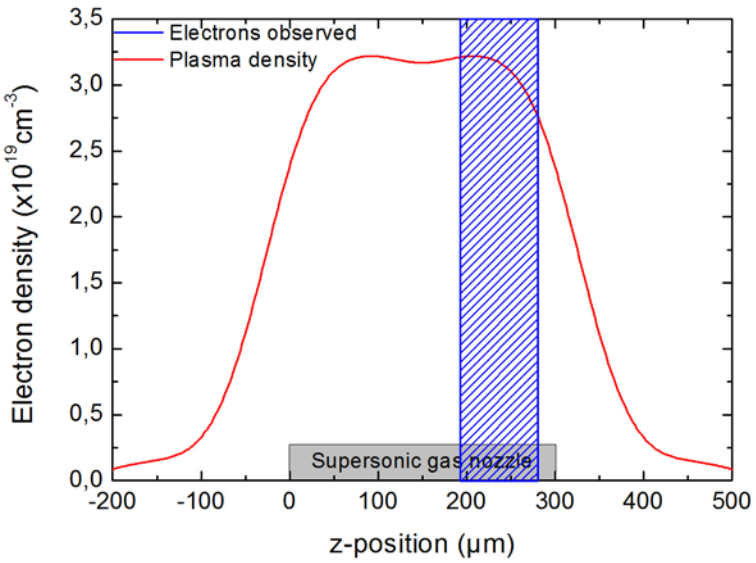

Figure 5. Electron plasma density profile (red) at the position of the plasma channel generated by the laser pulse. The position of the exit of the supersonic helium gas nozzle is indicated. The range, where electrons and so Faraday signal are observed in Fig. 4 are marked (blue area).

4. CONCLUSIONS

In conclusion, we have developed and applied techniques to characterize the charge, spectrum, pointing, divergence, transverse emittance of electron bunches. The most distinguished study is the real-time observation of the magnetic field of a laser accelerated electron bunch with unprecedented spatial and temporal (few-fs) resolution and the accelerator plasma wave at the same time by the combination of polarimetry and plasma shadowgraphy. Therefore, the first direct observation of the acceleration process is obtained with the temporal structure of the accelerated electron pulse encoded in the signal. The position of a single electron pulse inside of the plasma wave was determined to be in the first oscillation behind the driving laser pulse. An electron bunch duration of 5.8 fs FWHM was inferred from these results, confirming the expected ultra-short-duration.

ACKNOWLEDGMENT

We thank M. Geissler for providing us with the ILLUMINATION code to perform the PIC simulations. This work is supported by DFG-Project Transregio TR18, by the Association EURATOM, Max-Planck-Institut für Plasmaphysik, by the Munich Centre for Advanced Photonics (MAP), by Laserlab-Europe/Labtech FP7 contract number 228334 and by the German Ministry of Education and Research (BMBF) under contract 03ZIK052. C. M. S. S. acknowledges the support of the Alexander von Humboldt Foundation. J. M. M. acknowledges the support of the Alexander von Humboldt Foundation and the Russian Foundation for Basic Research (RFBR), grant numbers 08-02-01245-a and 08-02-01137-a.

REFERENCES

[1] T. Tajima, J. M. Dawson, "Laser electron accelerator," Phys. Rev. Lett. 43, 267 (1979).

[2] C. G. R. Geddes et al., "High-quality electron beams from a laser wakefield accelerator using plasma-channel guiding," Nature (London) 431, 538 (2004).

[3] S. P. D. Mangles et al., "Monoenergetic beams of relativistic electrons from intense laser–plasma interactions," Nature (London) 431, 535 (2004).

[4] J. Faure et al., "A laser–plasma accelerator producing monoenergetic electron beams," Nature (London) 431, 541 (2004).

[5] W. P. Leemans et al., "GeV electron beams from a centimetre-scale accelerator," Nature Phys. 2, 696-699 (2006).

[6] J. Faure et al., "Controlled injection and acceleration of electrons in plasma wakefields by colliding laser pulses," Nature (London) 444, 737 (2006).

[7] J. Van Tilborg et al., "Temporal characterization of femtosecond laser-plasma-accelerated electron bunches using terahertz radiation," Phys. Rev. Lett. 96, 014801 (2006).

[8] T. Ohkubo et al., "Temporal characteristics of monoenergetic electron beams generated by the laser wakefield acceleration," Phys. Rev. Spec. Top. Accel. Beams 10, 031301 (2007).

[9] J. Van Tilborg et al., "Single-shot measurement of the spectral envelope of broad-bandwidth terahertz pulses from femtosecond electron bunches," Opt. Lett. 33, 1186-1188 (2008).

[10] A. D. Debus et al., "Electron bunch length measurements from laser-accelerated electrons using single-shot THz time-domain interferometry," Phys. Rev. Lett. 104, 084802 (2010).

[11] O. Lundh et al., "Few femtosecond, few kiloampere electron bunch produced by a laser–plasma accelerator," Nature Phys. 7, 219-222 (2011).

[12] N. H. Matlis et al., "Snapshots of laser wakefields," Nature Phys. 2, 749-753 (2006).

[13] P. Dong et al., "Formation of optical bullets in laser-driven plasma bubble accelerators," Phys. Rev. Lett. 104, 134801 (2010).

[14] K. Schmid et al., "Few-cycle laser-driven electron acceleration," Phys. Rev. Lett. 102, 124801 (2009).

[15] A. Buck et al., "Absolute charge calibration of scintillating screens for relativistic electron detection," Rev. Sci. Instrum., 81, 033301 (2010).

[16] C. M. S. Sears et al., "A high resolution, broad energy acceptance spectrometer for laser wakefield acceleration experiments," Rev. Sci. Instrum., 81, 073304 (2010).

[17] C. M. S. Sears et al., "Emittance and divergence of laser wakefield accelerated electrons," Phys. Rev. ST Accel. Beams 13, 092803 (2010).

[18] J. A. Stamper & B. H. Ripin, "Faraday-rotation measurements of megagauss magnetic fields in laser-produced plasmas," Phys. Rev. Lett. 34, 138-141 (1975).

[19] M. C. Kaluza et al., "Measurement of magnetic-field structures in a laser-wakefield accelerator," Phys. Rev. Lett. 105, 115002 (2010).

[20] G. S. Settles, [Schlieren and Shadowgraph Techniques], Springer, (2001).

[21] D. Herrmann et al., "Generation of sub-three-cycle, 16 TW light pulses by using noncollinear optical parametric chirped-pulse amplification," Opt. Lett. 34, 2459-2461 (2009).

[22] M. Geissler, J. Schreiber, and J. Meyer-ter-Vehn, "Bubble acceleration of electrons with few-cycle laser pulses," New J. Phys. 8, 186 (2006).

[23] A. Buck et al., "Real-time observation of laser-driven electron acceleration," Nature Phys., doi:10.1038/nphys1942 (2011).